Energy management strategy for series-parallel hybrid electric tractors during traction operations

Mengnan Liu[1,2,3*], Shenghui Lei[1,2], Xianghai Yan[1,2], Yanying Li[1,2], Junjiang Zhang[1,2], Liyou Xu[1,2]

(1. *College of Vehicle and Traffic Engineering, Henan University of Science and Technology, Luoyang 471003, Henan, China*;
2. *State Key Laboratory of Intelligent Agricultural Power Equipment, Luoyang 471039, Henan, China*;
3. *YTO Group Corporation R&D Center, Luoyang 471039, Henan, China*)

Abstract: As agricultural modernization advances and environmental awareness grows, enhancing the energy efficiency and environmental performance of tractors, a core component of agricultural machinery, becomes a crucial research focus. This study centers on the series-parallel hybrid electric tractor (SPHET), analyzing its drive system structural characteristics and operational modes. The research involves developing a dynamic model for the hybrid electric tractor (HET) traction operations and proposing a real-time energy management strategy based on fuzzy logic rules (FLR). To precisely evaluate the superiority for real-time control strategies, an Energy Management Strategy based on final state-constrained dynamic programming (FSCDP) is introduced. To validate the feasibility and continuous power output capability of the proposed real-time control strategies, a hardware-in-the-loop (HIL) simulation platform for the SPHET energy management control strategy is established. Simulation results under plowing conditions show that, with the initial state of charge (SOC) of the battery set at 50%, the FLR control strategy reduces fuel consumption by 6.05% compared to the deterministic rule (DR) control strategy, resulting in a 0.57% increase in SOC. When compared with the FSCDP control strategy, both control strategies achieve the same final SOC value, and the fuel consumption of the FLR control strategy reaches 96.6% of the FSCDP level. This indicates that the energy management strategy based on FLR can effectively reduce energy consumption and is suitable for real-time application. For initial SOC values set at 30% or 80%, the FLR control strategy demonstrates lower energy consumption compared to DR. Both strategies ensure the power battery pack stays within the set upper and lower limits, ensuring the safe operation of the power battery pack while meeting continuous power demands under plowing conditions. The study results provide valuable insights and guidance for energy management in SPHET, contributing positively to the advancement of sustainable mechanized agriculture.

Keywords: hybrid electric tractor, fuzzy logic, dynamic programming, energy management strategy, hardware-in-the-loop simulation

DOI: 10.25165/j.ijabe.20261901.8796

Citation: Liu M N, Lei S H, Yan X H, Li Y Y, Zhang J J, Xu L Y. Energy management strategy for series-parallel hybrid electric tractors during traction operations. Int J Agric & Biol Eng, 2026; 19(1): 76–87.

1 Introduction

In the face of escalating environmental degradation and resource scarcity, research on energy-efficient and environmentally friendly agricultural tractors with new power technologies has become increasingly crucial[1-6]. Confronted with challenges and constraints such as battery acquisition costs, lifespan, and energy density, the development of hybrid electric tractors that combine the advantages of traditional fuel tractors and pure electric tractors has emerged as an innovative direction to reduce fuel consumption and exhaust emissions[7,8]. From the perspective of energy hybridization, hybrid electric tractors can be categorized into series, parallel, and series-parallel structures[9]. Among them, the SPHET integrates the advantages of both series and parallel structures, balancing tractor power performance, fuel consumption, and emission requirements. This is particularly significant for regions in the agricultural industry that do not yet have a fully established infrastructure for new energy sources[1].

For HET, energy management strategy plays a crucial role in coordinating the power distribution of different power sources. This strategy is typically categorized into three major classes: rule-based, optimization-based, and learning-based approaches[10,11].

Rule-based energy management strategies consist of methods based on DR and FLR[12]. Xu et al.[13] developed a DR-based strategy for a range-extender hybrid electric tractor, adjusting control parameters to significantly reduce fuel consumption compared to fixed-point strategies. Kang et al.[14] proposed an energy management strategy for a plug-in series hybrid electric tractor (SHET) based on charge depletion and sustaining rules, studying the battery state of charge variations under various operating conditions. Lee et al.[15] introduced DR-based energy management strategies for a parallel hybrid electric tractor (PHET), conducting simulation comparisons that showed an efficiency improvement of 11.78% compared to traditional fuel tractors and 1.88% over DR energy management strategies. Jia et al.[16] designed and studied two

Received date: 2024-01-08 **Accepted date:** 2025-12-25

Biographies: Shenghui Lei, PhD candidate, research interest: drivetrain and intelligent control technology for tractors, Email: leishenghui95@163.com; **Xianghai Yan**, PhD, Associate Professor, research interest: tractor transmission control and testing technology, Email: 9905167@haust.edu.cn; **Yanying Li**, PhD candidate, research interest: drivetrain and intelligent control technology for tractors, Email: lyy_1997@outlook.com; **Junjiang Zhang**, PhD, Associate Professor, research interest: electric vehicle design and control, Email: zhangjunjiang2020@163.com; **Liyou Xu**, PhD, Professor, research interest: vehicle transmission theory and control technology, Email: xlyou@haust.edu.cn.

***Corresponding author: Mengnan Liu**, PhD, Researcher, research interest: drivetrain and intelligent control technology for tractors. YTO Group Corporation R&D Center, Luoyang 471039, China, Tel: +86-379-62690333, Email: liumengnan27@163.com.

DR energy power management strategies for a benchmark-based SHET, namely a thermostat and a power follower controller. Simulation results based on typical working cycles indicated that the power follower controller achieved better performance in fuel savings and emission reduction, albeit with the drawback of increased particulate matter. Wang et al.[17] investigated a power-following control strategy for an extended-range electric tractor, establishing a forward predictive control model for motor power. Simulation analysis demonstrated improvements in low-speed tracking, acceleration response, and high-speed range extender starting characteristics, with the lag in predicted power favoring stable range extender operation and smooth unloading. Mocera et al.[18,19] designed a numerical model for a PHET, defining an energy management control strategy primarily utilizing an internal combustion engine with motor assistance. The performance of the parallel hybrid powertrain structure was studied based on a set of tasks characteristic of real orchard tractors, resulting in an average energy consumption reduction of 16% compared to traditional thermal power units. Subsequently, a power split hybrid electric tractor was proposed, introducing two control strategies for battery depletion and battery sustainment, followed by simulation analysis. Rossi et al.[20] introduced a hybrid powertrain transmission for agricultural tractors based on an electrically driven continuously variable transmission. They formulated the fundamental control strategy for the transmission's full hybrid mode based on changes in vehicle speed. Wu et al.[21] established a FLR energy management strategy for an extended-range electric tractor, introducing dynamic SOC correction factors during the battery maintenance phase and optimizing the fuzzy control rules using the non-dominated sorting genetic algorithm II. The proposed fuzzy improvement strategy extended battery life by 2131.9 seconds and reduced SOC by 7.21%.

Optimization-based methods can be further categorized into offline optimization control and transient optimization control[10]. Pontryagin's Minimum Principle, genetic algorithms, and Dynamic Programming (DP) algorithms are often used for offline optimization control. Typical methods for transient optimization control include model predictive control strategies and equivalent consumption minimization strategies. Dou et al.[22] proposed a machine-coupled split powertrain tractor configuration, introducing an energy management strategy based on predicted demand power, resulting in an 8.0% equivalent fuel consumption reduction in rotary tillage mode compared to rule-based control strategies. Zhang et al.[23,24] selected a parallel hybrid diesel-electric hybrid electric tractor as the research subject and established an energy-saving control strategy based on Pontryagin's Minimum Principle. When compared with a control strategy based on the optimal economic curve, under rotary tillage conditions, the equivalent fuel consumption was reduced by 10.44%, and under plowing conditions, the equivalent fuel consumption decreased by 11.20%. Subsequent research combined power output prediction methods, trajectory tracking methods, and a real-time energy-saving control method based on instantaneous optimization with speed and power output as interactive variables. Wang et al.[25] studied a dual-motor independent electric drive extended-range electric tractor rotary tillage system, performing simulation experiments and bench tests based on the dynamic programming algorithm. The simulation test results closely matched the bench test results, with a relative error of 1.77%. Zhu et al.[26] proposed an adaptive equivalent fuel consumption minimization strategy for an electromechanical-hydraulic hybrid electric tractor fused with working condition predictions. Compared to the equivalent consumption minimization strategy with fixed equivalent factors and the adaptive equivalent fuel consumption minimization strategy based solely on SOC feedback, tractor fuel consumption decreased by 6.30% and 2.55% respectively under plowing conditions.

With the development of big data, artificial intelligence, and computer technology, machine learning has been actively applied to energy management problems, providing a research avenue to overcome the limitations of traditional methods[11]. However, given the complexity of tractor operations and the variability in agricultural machinery, the cost of learning is substantial, leading to a lack of prominent research in this area for the time being.

In summary, the current focus of research on HET is predominantly on series and parallel configurations, with limited attention to series-parallel configurations. Furthermore, findings from a market potential survey for HET indicate that farmers consider reliability a decisive factor in their purchase decisions[27]. In other words, the stability and reliability of the HET control system stand out as primary considerations in the design of control algorithms. Presently, rule-based energy management strategies serve as the primary approach for real-time control of HET power systems. Concerning global optimization control methods, the prerequisite of having prior knowledge of total drive power demand is exceptionally challenging in practical applications. Therefore, global optimal control is typically implemented offline and serves as a benchmark for exploring the potential fuel economy[28,29]. As for transient optimization control, the computational complexity of online optimization strategies exhibits an exponential increase with the addition of constraints, model accuracy, and problem discretization. This trend leads to a significant rise in control costs[12,30].

This paper focuses on the study of a series-parallel configuration of HET, analyzing its drive system structure characteristics and operational modes. A dynamic model for the traction operation of the SPHET is constructed. Building upon this foundation, a real-time energy management strategy based on FLR is proposed. To more accurately assess the superiority of real-time control strategies, an Energy Management Strategy based on FSCDP is introduced. To validate the rationality of the proposed real-time control strategy and the sustained power output capability of the SPHET, an HIL simulation platform for the energy management control strategy of the SPHET is established. Simulation comparisons of different energy management strategies are conducted under plowing conditions. This study represents significant progress in the modeling and energy management of SPHET, providing valuable insights for future research in this field.

The remaining sections of this paper are outlined as follows. Section 2 presents the dynamic model for the traction operation of the SPHET. Section 3 introduces two energy management strategies, namely based on FLR and based on FSCDP. Section 4 validates and analyzes the proposed strategies through the HIL simulation platform. Section 5 provides the conclusions drawn from the study.

2 Establishment of an SPHET model

2.1 Structural configuration

This passage describes a hybrid SPHET drive system configuration, as illustrated in Figure 1. The engine is directly connected to the rotor of P1 motor, and it is also connected to the rotor of P2 motor through a reversing device. The power coupled from the power source can be transmitted to the agricultural

implement through the power take-off (PTO) transmission device and to the drive axle through the transmission device.

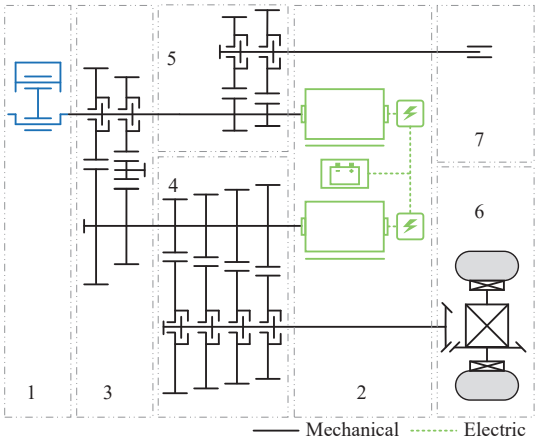

1. Engine 2. Electric drivetrain; 3. Reversing device 4. Transmission device 5. PTO transmission device 6. Drive axle and wheels 7. Agricultural implement

Figure 1 The configuration of drive system for SPHET

This paper takes the Dongfanghong 1804 wheeled tractor as the research subject. The main components of the SPHET are selected based on its operating conditions, and specific parameters are detailed in Table 1[31,32].

Table 1 Key technical parameters of the SPHET

Components	Parameters	Values
Engine	Rated power/kW	132.5
	Maximum torque/N·m	771
P1 motor	Continuous power/kW	84
	Continuous torque/N·m	500
P2 motor	Continuous power/kW	100
	Continuous torque/(N·m)	400
Power battery	Rated capacity/A·h	50
	Rated voltage/V	532.8
Mechanical transmission system	Reversing device (F, R)	0.85, 1
	Transmission device (Ⅰ, Ⅱ, Ⅲ, Ⅳ)	2.96, 1.93, 1.26, 0.83
	PTO transmission device (Ⅰ, Ⅱ)	1.60, 2.91
	Drive axle (F, R)	32.65, 25.52
	Mechanical transmission efficiency	0.9

2.2 Engine model

Ignoring the engine dynamics, the brake specific fuel consumption (BSFC) of the engine can be considered as a function of engine torque and speed. Therefore, this paper establishes a quasi-static interpolation model based on data obtained from bench tests. This model, within a certain accuracy range, reflects the characteristics of the engine[33]. The BSFC of the engine is expressed as follows:

$$b_e = f_b(T_e, n_e) \tag{1}$$

where, T_e is the engine output torque, N·m; n_e is the engine output speed, r/min; b_e is the BSFC of engine, g/(kW·h).

The fuel consumption is calculated using the interpolated fuel consumption rate, which is determined according to the following equation:

$$L_e = \frac{1}{3.438\times10^{10}\times\rho_e}\int_{t_0}^{t_1} T_e n_e b_e \mathrm{d}t \tag{2}$$

where, t_0 is the engine start time, s; t_1 is the engine stop time, s; L_e is the engine fuel consumption, L; ρ_e is diesel density, g/mL.

2.3 Electric drivetrain model

2.3.1 Motor model

The efficiency of the electric motor is established by utilizing bench test data through interpolation modeling. The model for motor efficiency is expressed as follows:

$$\eta_{x\mathrm{M}} = f_{x\mathrm{M}\eta}(T_{x\mathrm{M}}, n_{x\mathrm{M}}) \tag{3}$$

where, x represents P1 motor when it is P1 and represents P2 motor when it is P2; $T_{x\mathrm{M}}$ is the motor output torque, N·m; $n_{x\mathrm{M}}$ is the motor output speed, r/min; $\eta_{x\mathrm{M}}$ is the motor efficiency.

The power at the input of the motor is calculated using the following equation:

$$P_{x\mathrm{M}} = \frac{T_{x\mathrm{M}} n_{x\mathrm{M}} \eta_{x\mathrm{M}}^{-\mathrm{sgn}(T_{x\mathrm{M}})}}{9550} \tag{4}$$

where, $P_{x\mathrm{M}}$ is the power at the motor input, kW.

2.3.2 Battery model

By equivalently modeling the power battery pack as a series circuit comprising an open-circuit voltage and an internal resistance, the mathematical equations are straightforward, facilitating computational modeling[34]. To simplify the modeling process, the nonlinear variations of the power battery pack's open-circuit voltage and internal resistance with SOC were measured at room temperature, as illustrated in Figure 2. The battery output current is defined as a function of the required battery pack power, internal resistance, and open-circuit voltage.

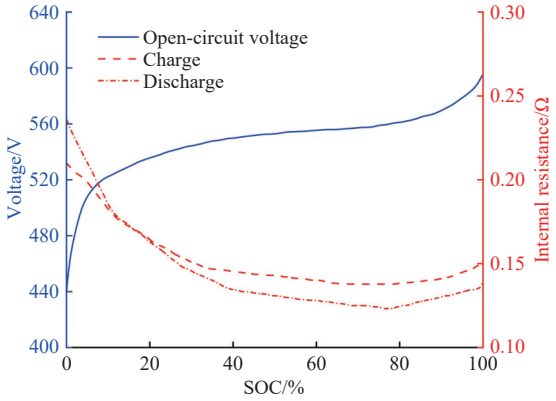

Figure 2 Charge/discharge internal resistance and open circuit voltage of battery pack

$$\begin{cases} U_{\mathrm{bp}} = U_{\mathrm{oc}} - R_{\mathrm{bp}} I_{\mathrm{bp}} \\ P_{\mathrm{bp}} = U_{\mathrm{bp}} I_{\mathrm{bp}} \\ I_{\mathrm{bp}} = \dfrac{U_{\mathrm{oc}} - \sqrt{U_{\mathrm{oc}}^2 - 4P_{\mathrm{bp}}R_{\mathrm{bp}}}}{2R_{\mathrm{bp}}} \end{cases} \tag{5}$$

where, U_{bp} is the battery pack voltage, V; U_{oc} is the open-circuit voltage of the battery pack, V; I_{bp} is the battery pack output current, A; R_{bp} is the charge-discharge internal resistance of the battery pack, Ω; P_{bp} is battery pack power, W.

Determine the SOC for the battery pack through ampere-hour integration.

$$\mathrm{SOC}_{t_b} = \mathrm{SOC}_0 - \frac{1}{Q_{\mathrm{bp}}}\int_0^{t_b} I_{\mathrm{bp}} \mathrm{d}t \tag{6}$$

where, SOC_{t_b} is the SOC of the battery pack at time t_b; SOC_0 is the initial SOC of the battery pack; Q_{bp} is the rated capacity of the battery pack, A·h; t_b is the charging or discharging time of the battery pack, s.

2.4 Mechanical drivetrain model

According to the engagement or disengagement of the clutches in the reversing device, transmission shaft, and variable-speed device, there are different connection modes between the engine, P1 motor, P2 motor, and the drive wheels. This leads to various dynamic and kinematic relationships:

$$\begin{cases} F_{\mathrm{D}} = \dfrac{((T_{\mathrm{e}}+T_{\mathrm{P1M}})C_{\mathrm{fb}}i_{\mathrm{fb}}+T_{\mathrm{P2M}})C_{gn}i_{gn}i_{\mathrm{da}}\eta_{\mathrm{t}}}{r_{\mathrm{w}}} \\ v_{\mathrm{a}} = 0.377\dfrac{C_{gn}r_{\mathrm{w}}n_{\mathrm{P2M}}\eta_{\mathrm{S}}}{i_{gn}i_{\mathrm{da}}} = 0.377\dfrac{C_{gn}C_{\mathrm{fb}}r_{\mathrm{w}}n_{\mathrm{e}}\eta_{\mathrm{S}}}{i_{\mathrm{fb}}i_{gn}i_{\mathrm{da}}} = \\ \quad 0.377\dfrac{C_{gn}C_{\mathrm{fb}}r_{\mathrm{w}}n_{\mathrm{P1M}}\eta_{\mathrm{S}}}{i_{\mathrm{fb}}i_{gn}i_{\mathrm{da}}} \end{cases} \tag{7}$$

where, F_{D} is the total driving force of the tractor, N; v_{a} is the actual speed of the tractor, km/h; C_{fb} is the clutch state coefficient of the reversing device, combined is equal to 1, and disconnected is equal to 0; C_{gn} is the clutch state coefficient of the variable-speed device; r_{w} is the wheel radius, m; η_{S} is the slip efficiency; η_{t} is the mechanical transmission system efficiency; i_{fb} is the transmission ratio of the reversing device; i_{gn} is the transmission ratio of the variable-speed device; i_{da} is the drive axle gear ratio.

2.5 Tire soil interaction model

The mathematical model for traction prediction can capture the intricate relationship between the driving performance of tractor tires and soil characteristics[35].

$$\begin{cases} B_{\mathrm{n}i} = \dfrac{CIb_id_i(1+5d_{\mathrm{c}i}/h_i)}{F_{zi}(1+3b_i/d_i)} \\ GTR_i = \dfrac{F_{\mathrm{w}i}}{F_{zi}} = 0.88(1-e^{-0.08B_{\mathrm{n}i}})(1-e^{-7S_i})+0.03 \\ MRR_i = \dfrac{F_{\mathrm{m}i}}{F_{zi}} = \dfrac{1.2}{B_{\mathrm{n}i}}+\dfrac{0.5S_i}{\sqrt{B_{\mathrm{n}i}}}+0.03 \end{cases} \tag{8}$$

where, B_{n} is the tire traction index; i represents front wheels when it is f and represents rear wheels when it is r; CI is the tire-soil cone index; b is the unloaded tire section width, m; d is the unloaded tire diameter, m; d_{c} is the tire radial deformation, m; h is the tire section height, m; F_{z} is the tire normal load, N; GTR is the tire traction utilization coefficient; F_{w} is the tire traction force, N; S is the tire slip ratio; MRR is the tire rolling resistance coefficient; F_{m} is the tire motion resistance, N.

Figure 3 depicts the traction force analysis of a four-wheel drive tractor. Assuming the tractor's center of mass coordinates and the extension line of the traction force are in the same plane perpendicular to the ground, the load on the driving wheels on both sides of the same drive axle is equal. Subsequently, torque balance equations for both the front and rear drive axles will be outlined.

$$\begin{cases} F_{\mathrm{Ar}} = \dfrac{mg(L-a+e_{\mathrm{f}})+F_{\mathrm{T}}h_{\mathrm{T}}}{L-e_{\mathrm{r}}+e_{\mathrm{f}}} = 2F_{\mathrm{zr}} \\ F_{\mathrm{Af}} = \dfrac{mg(a-e_{\mathrm{r}})-F_{\mathrm{T}}h_{\mathrm{T}}}{L-e_{\mathrm{r}}+e_{\mathrm{f}}} = 2F_{\mathrm{zf}} \end{cases} \tag{9}$$

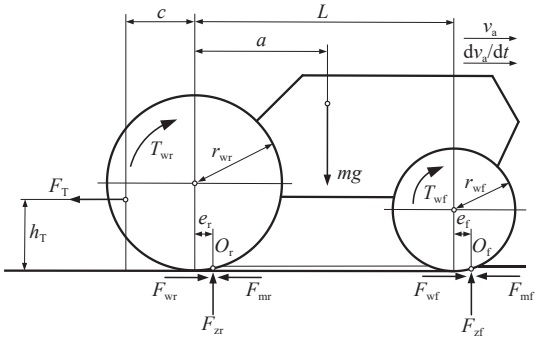

Figure 3 Longitudinal dynamics for the four-wheel drive tractor

where, F_{A} is the drive axle normal load, N; m is the tractor mass, kg; g is the acceleration due to gravity, $\mathrm{kg\cdot m/s^2}$; L is the tractor wheelbase, m; a is the longitudinal distance from the center of mass to the rear axle center, m; e is the wheel offset distance, m; F_{T} is the traction resistance of agricultural machinery, N; h_{T} is the towing point height, m.

According to Equation (8) and Equation (9), the total driving force and motion resistance of the four-wheel drive tractor can be calculated.

$$\begin{cases} F_{\mathrm{D}} = \sum\limits_{i=\mathrm{f,r}} GTR_iF_{\mathrm{A}i} \\ F_{\mathrm{M}} = \sum\limits_{i=\mathrm{f,r}} MRR_iF_{\mathrm{A}i} \end{cases} \tag{10}$$

where, F_{M} is the motion resistance, N.

After considering the mismatch in motion between the front and rear axles of the four-wheel drive tractor, slip and motion efficiency can be obtained[36].

$$\begin{cases} \eta_{\mathrm{S}} = \dfrac{F_{\mathrm{D}}}{2\left(\dfrac{F_{\mathrm{wf}}}{1-S_{\mathrm{f}}}+\dfrac{F_{\mathrm{wr}}}{1-S_{\mathrm{r}}}\right)} \\ \eta_{\mathrm{M}} = \dfrac{F_{\mathrm{D}}-F_{\mathrm{M}}}{F_{\mathrm{D}}} \end{cases} \tag{11}$$

where, η_{S} is the slip efficiency; η_{M} is the motion efficiency.

According to the traction performance prediction method for four-wheel drive tractors, the relationship between tractor slip efficiency, motion efficiency, and traction force can be obtained, as shown in Figure 4.

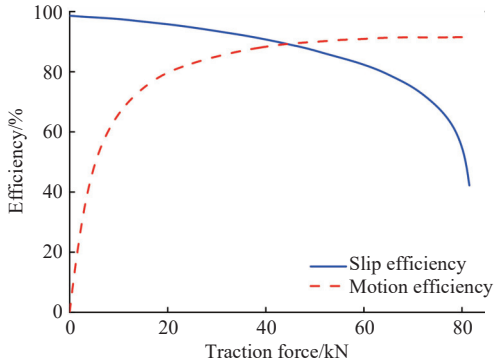

Figure 4 Slip and motion efficiency

2.6 Driver model

The driver model can realistically simulate the actual operation of the driver in forward simulation. The model can be represented as a PI controller with respect to the vehicle speed error. Its output is the throttle opening, denoted as θ, $\theta \geq 0$ representing the accelerator pedal opening, and $\theta < 0$ representing the brake pedal opening.

$$\theta = K_{\mathrm{P}}(v_{\mathrm{t}}-v_{\mathrm{a}})+K_{\mathrm{I}}\int(v_{\mathrm{t}}-v_{\mathrm{a}})\mathrm{d}t \tag{12}$$

where, θ is the pedal opening, $0^\circ \leq |\theta| \leq 100^\circ$; v_{t} is the target vehicle speed, km/h; K_{P} is the proportional coefficient; K_{I} is the integral coefficient.

2.7 Traction dynamics model

The tractor involved in the operation of moving the traction unit needs to overcome its own generated motion resistance while also overcoming the traction resistance generated by the passive agricultural implements. The driving force and the total resistance together determine the acceleration of the unit. The longitudinal

dynamic equation of the tractor under traction operation is established.

$$m\frac{\mathrm{d}v_a}{\mathrm{d}t}=F_D-F_M-F_T \tag{13}$$

3 Energy management strategy

3.1 Based on FLR

This article primarily focuses on the operation of the traction unit. As shown in Figure 5, three operation modes are defined: Pure Electric (PE), Series Hybrid (SH), and Parallel Hybrid (PH). In the PH mode, based on the state of the P2 motor, it can be further divided into three sub-modes: Pure Internal Combustion Engine (PICE), Parallel Hybrid Drive (PHD), and Parallel Hybrid Generation (PHG). As shown in Figure 6, to prevent frequent switching, SW_1 and SW_2 are set as the lower and upper bounds of the hysteresis zone for switching between PE/SH and PH modes. SW_3 and SW_4 are set as the lower and upper bounds of the hysteresis zone for switching between PE and SH modes. The arrows in the figure illustrate the switching mechanism. SW_5 and SW_6 are set as the limits for switching between PHD and PICE modes and the limits for switching between PICE and PHG modes.

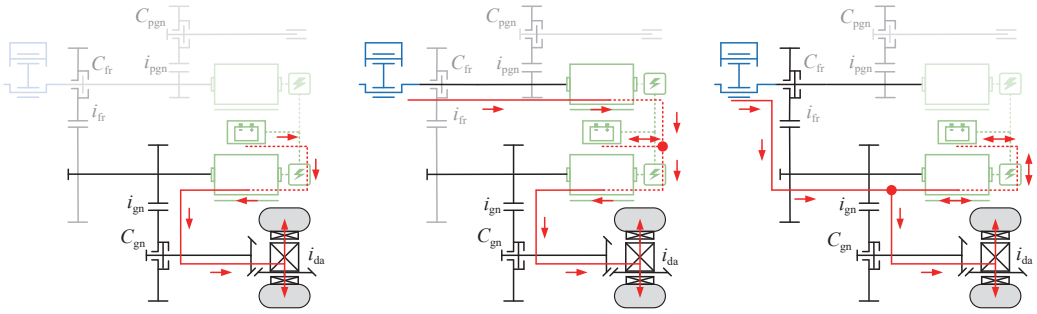

a. PE mode b. SH mode c. PH mode

Figure 5 Operation modes of traction unit for SPHET

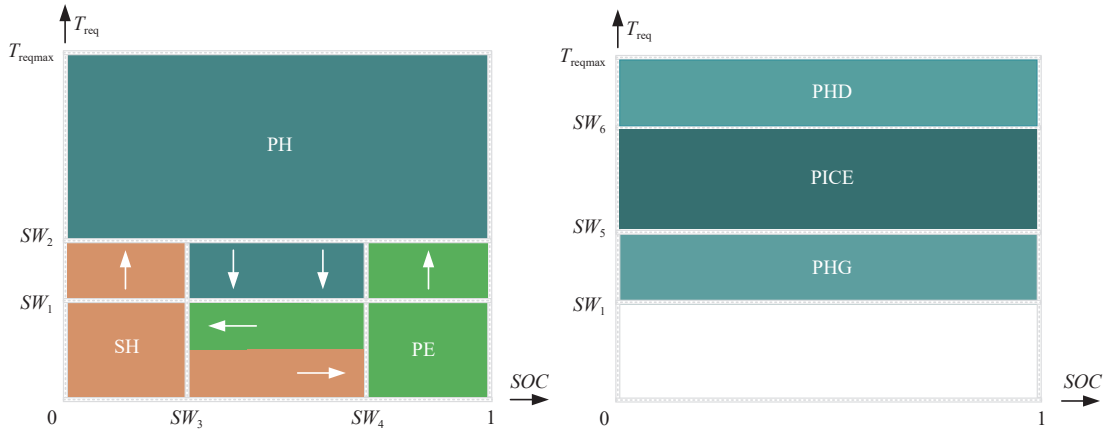

a. Switching between PE/SH and PH modes b. Switching between PICE, PHD, and PHG modes

Figure 6 Energy management strategy rules

The specific rules for operation modes and torque distribution are as follows:

(1) In the PE mode, when $SW_3 \le \mathrm{SOC} \le 1$ and $0 < T_{req} < SW_2$ are true, the engine and P1 motor are turned off, and the P2 motor is turned on. The vehicle is solely driven by the P2 motor, and all the driving power comes from the traction battery. The energy flow is illustrated in Figure 5a. When $0 \le \mathrm{SOC} < SW_3$ and $0 < T_{req} < SW_2$ are true, the system switches to the SH mode. When , the system switches to the PH mode.

$$\begin{cases} T_e=0 \\ T_{P1M}=0 \\ T_{P2M}=\min(T_{req}/i_{fb},\ T_{P2MC}) \end{cases} \tag{14}$$

where, T_{P2MC} is the continued torque from the P2 motor, N·m.

(2) In the SH mode, when $0 \le \mathrm{SOC} < SW_3$ and $0 < T_{req} < SW_2$ are true, the engine, P1 motor, and P2 motor are all started. The engine drives the P1 motor to provide power to the battery or the P2 motor. The P2 motor operates independently, and the driving power comes from both the traction battery and the engine. The energy flow is illustrated in Figure 5b. When $SW_4 \le \mathrm{SOC} \le 1$ and $0 < T_{req} < SW_2$ are true, the system switches to the PE mode. When $T_{req} \ge SW_2$, the system switches to the PH mode.

$$\begin{cases} T_e=T_{eSHopt} \\ T_{P1M}=-T_e \\ T_{P2M}=\min(T_{req}/i_{fb},\ T_{P2MC}) \end{cases} \tag{15}$$

where, T_{eSHopt} is the optimal torque in the SH mode of the engine, N·m.

(3) In the PH mode, when $SW_2 < T_{req} \le T_{reqmax}$ are true, the engine and P2 motor are started, while the P1 motor is turned off. The engine and P2 motor jointly drive the system, and the driving power comes from both the traction battery and the engine. The energy flow is illustrated in Figure 5c. When $0 \le \mathrm{SOC} < SW_4$ and $T_{req} < SW_1$ are true, the system switches to the SH mode. When $SW_4 \le \mathrm{SOC} \le 1$ and $T_{req} < SW_1$ are true, the system switches to the PH mode.

$$\begin{cases} T_{\text{ePHD}}=SW_6, & T_{\text{req}} \geq SW_6 \\ T_{\text{ePICE}}=T_{\text{reqe}}, & SW_5 < T_{\text{req}} < SW_6 \\ T_{\text{ePHG}}=SW_5, & T_{\text{req}} \leq SW_5 \end{cases} \tag{16}$$

where, T_{ePHD} is the engine output torque in PHD mode, N·m; T_{ePICE} is the engine output torque in PICE mode, N·m; T_{ePHG} is the engine output torque in PHG mode, N·m.

$$\begin{cases} T_{\text{e}} = (T_{\text{ePHD}}, T_{\text{ePICE}}, T_{\text{ePHG}}) \\ T_{\text{P1M}}=0 \\ T_{\text{P2M}}=\min((T_{\text{req}}-T_{\text{e}})/i_{\text{fb}}, T_{\text{P2MC}}) \end{cases} \tag{17}$$

According to the characteristics of the power battery and the operational features of the tractor, the minimum torque curve of the engine in the high-efficiency area, the equivalent curve of the rated torque of the P2 motor, and the lower and upper limits of SOC are selected as the setpoints SW_1, SW_2, SW_3, and SW_4, respectively. Selecting the minimum torque curve in the high-efficiency area of the engine and the engine external characteristic curve are selected as the reference values for SW_5 and SW_6.

Due to the complex and varying load conditions during tractor traction operations, the loads of different implements exhibit a stable normal distribution within a certain range as random loads. In PH mode, SW_5 and SW_6 determine the energy-saving effect of the tractor and the variation of SOC during load operation.

To ensure the HET can consistently maintain power performance and improve the fuel economy of the tractor, fuzzy logic is introduced on top of the determined rule benchmark values, replacing fixed rules. This allows for adjustments to the rules to enhance control flexibility. The equivalent factor T_{reqeq} and SOC are selected as the two input variables, where x_1 and x_2 represent the proportion coefficients SW_5 and SW_6 of the baseline values as two output variables. Define "positive large (PB)", "positive small (PS)", "zero (ZR)", "negative small (NS)", and "negative large (NB)" as five linguistic variables to describe the variation of T_{reqeq}, SOC, x_1, and x_2. Using the triangular function as the affiliation function, the theoretical domain of T_{reqeq} is set to {1.5, 2.25, 3, 3.75, 4.5}; the theoretical domain of SOC is set to {0.3, 0.425, 0.55, 0.675, 0.8}; the theoretical domain of x_1 is set to {0.8, 0.85, 0.9, 0.95, 1}; the theoretical domain of x_2 is set to {1, 1.2, 1.4, 1.6, 1.8}. The fuzzy logic rules are listed in Table 2.

Table 2 Fuzzy logic rules table

x_1, x_2		T_{req}				
		NB	NS	ZE	PS	PB
SOC	NB	ZE/PS	PS/PB	PB/PB	PB/PB	PB/PB
	NS	NS/ZE	ZE/PS	PS/PB	PB/PB	PB/PB
	ZE	NB/NS	NS/ZE	ZE/PS	PS/PB	PB/PB
	PS	NB/NB	NB/NS	NS/ZE	ZE/PS	PS/PB
	PB	NB/NB	NB/NB	NB/NS	NS/ZE	ZE/PS

$$\begin{cases} SW_5 = \min(x_1 T_{\text{eoptd}}, T_{\text{eopt}}) \\ SW_6 = \max(x_2 T_{\text{eoptu}}, T_{\text{eopt}}) \end{cases} \tag{18}$$

where, T_{eoptd} is the curve value under the optimal working range torque of the engine, N·m; T_{eopt} is the optimal working torque curve value of the engine, N·m; T_{eoptu} is the curve value on the optimal working range torque of the engine, N·m.

3.2 Based on FSCDP

DP can effectively handle constraints and nonlinear problems, finding global optimal solutions[37]. The energy management problem of HET can be simplified to a nonlinear discrete system optimization problem over N stages, with the system equations shown as follows:

$$\begin{cases} x_{k+1} = f(x_k, u_k), & k = 0, 1, ..., N-1 \\ x(0) = x_0 \\ x_k \in X_k \\ u_k \in U_k \end{cases} \tag{19}$$

where, x_{k+1} is the system state variables at time step $k+1$; x_k is the system state variables at time step k; N is the number of stages in the discretized time domain for the target operating condition; x_0 is the initial values of the system; X_k is the feasible domain of the system's state variables at time k; u_k is the control variables of the system at time k; U_k is the feasible domain of the control variables of the system at time k.

For SPHET, the focus of the optimization objective is primarily on the vehicle's fuel economy. Therefore, the energy management problem based on dynamic programming becomes a problem of finding the control sequence for the hybrid power system that minimizes the cost function.

$$J = \sum_{k=0}^{N-1} L_{\text{e}}(x_k, u_k) \tag{20}$$

where, J is the total fuel consumption during the optimization process, L; $L_{\text{e}}(x_k, u_k)$ is the instantaneous fuel consumption of the system in stage k, L.

In order to ensure the normal operation of each subsystem, the following constraints need to be satisfied:

$$\begin{cases} \text{SOC}_{\min} \leq \text{SOC}_k \leq \text{SOC}_{\max} \\ n_{\text{emin}} \leq n_{\text{ek}} \leq n_{\text{emax}} \\ T_{\text{emin}}(\omega_{\text{ek}}) \leq T_{\text{ek}} \leq T_{\text{emax}}(\omega_{\text{ek}}) \\ n_{\text{P1Mmin}} \leq n_{\text{P1M}k} \leq n_{\text{P1Mmax}} \\ T_{\text{P1Mmin}}(n_{\text{P1M}k}, \text{SOC}_k) \leq T_{\text{P1M}k} \leq T_{\text{P1Mmax}}(n_{\text{P1M}k}, \text{SOC}_k) \\ n_{\text{P2Mmin}} \leq n_{\text{P2M}k} \leq n_{\text{P2Mmax}} \\ T_{\text{P2Mmin}}(n_{\text{P2M}k}, \text{SOC}_k) \leq T_{\text{P2M}k} \leq T_{\text{P2Mmax}}(n_{\text{P2M}k}, \text{SOC}_k) \end{cases} \tag{21}$$

where, SOC is the State of Charge of the power battery pack, subscript 'min' denotes the minimum value of the variable, subscript 'max' denotes the maximum value of the variable, and subscript 'k' represents the current value of the variable.

According to the theory of DP, the multi-stage optimization problem of control strategy can be decomposed into a series of subproblems by utilizing a backward approach to find the minimum cost function. In the reverse solving process, the problem described by Equation (19) is transformed into Equations (22) and (23).

The subproblem of step $N-1$:

$$J_{N-1}^*(x_{N-1}) = \min_{u_{N-1}}[L(x_{N-1}, u_{N-1})] \tag{22}$$

The subproblem of step k $(0 \leq k \leq N-1)$:

$$J_k^*(x_k) = \min_{u_k}[L(x_k, u_k) + J_{k+1}^*(x_{k+1})] \tag{23}$$

After obtaining the optimal control path for each state variable at the initial time, starting from the target initial state, forward calculation is performed based on the correspondence between state variables and optimal control variables at each time, which allows the determination of the optimal solution for the cost.

Based on the adopted configuration of the SPHET propulsion system, this paper selects the battery SOC as the state variable. In

different modes, the working engine, P1 motor, and P2 motor are all coupled with the road. Therefore, the engine torque and gearbox gear position are selected as control variables. To prevent the dynamic programming algorithm from falling into the 'curse of dimensionality,' in the SH mode, the speed of P1 motor is set to 1600 rpm according to efficiency[38]. The selected state variables, control variables, and grid division in DP are listed in Table 3.

Table 3 State and control variables in DP

Variable	Variable name	Grid partitioning
State	SOC	[0.3:0.005:0.8]
Control 1	Engine torque ratio	[0:0.01:1]
Control 2	Working mode	[1, 2, 3]
Control 3	Gear position	[1, 2, 3, 4]

To more accurately assess the superiority of real-time control strategies, this paper will employ a dynamic programming approach based on an optimization problem with terminal constraints[39-41]. By restricting the terminal conditions of the target state to a smaller range and leveraging the solutions provided in the literature, the adjustment capability for the terminal SOC state can be achieved.

According to Equation (6), Equation (19) can be reformulated as:

$$\begin{cases} x_{k+1} = F_k(x_k, u_k) + x_k, \quad k = 0, 1, ..., N-1 \\ F_k(x_k, u_k) = f_k(x_k, u_k) - x_k \end{cases} \tag{24}$$

The definition at time k, allowing the system to reach the minimum state variable value of the lower boundary of the terminal state, is denoted as the lower boundary constraint $x_{k,\text{low}}$ at that moment. According to the SOC terminal adjustment requirements of HET, the range of terminal state variables is a known quantity, i.e., $x_{N,\text{low}} = x_{\text{f,min}}$, where $x_{\text{f,min}}$ is the lower boundary of the terminal state. The lower boundary can be determined through backward iteration over time from $k = N-1$ to $k = 0$.

$$\begin{cases} x_{k,\text{low}} = \min\limits_{x_k, u_k} x_k \\ F_k(x_{k,\text{low}}, u_k) + x_{k,\text{low}} = x_{k+1,\text{low}} \\ x_{k,\text{low}} \in X_k \\ u_k \in U_k \end{cases} \tag{25}$$

In the backward iteration calculation, $x_{k+1,\text{low}}$ is a known quantity, while $x_{k,\text{low}}$ and u_k are unknown. Therefore, the solution for $x_{k,\text{low}}$ involves a fixed-point problem denoted as $(x = f(x))$, which can be solved using a fixed-point iteration method. If the state is assumed to be unconstrained, i.e., the following formulation is equivalent:

$$x_{k,\text{low}} = x_{k+1,\text{low}} - \max_{u_k \in U_k} F_k(\mathrm{x}_{k,\text{low}}, u_k) \tag{26}$$

The fixed point problem of time step k without state constraints can be solved with the following algorithm:

(1) Initialization:

$$x_{k,\text{low}}^{j=0} = x_{k+1,\text{low}} \tag{27}$$

where, j is the iteration index for calculating the lower bound of the state variables at time k.

(2) Iterative calculation until a specific tolerance is reached:

$$x_{k,\text{low}}^{j+1} = x_{k+1,\text{low}} - \max_{u_k \in U_k} \{F_k(\mathrm{x}_{k,\text{low}}^{j}, u_k)\} \tag{28}$$

The algorithm converges in the following cases:

$$\left| \frac{\partial}{\partial x_{k,\text{low}}^{j}} \max_{u_k \in U_k} \{F_k(\mathrm{x}_{k,\text{low}}^{j}, u_k)\} \right| < 1 \tag{29}$$

After completing the lower boundary calculation for time k, the same solving process is repeated to obtain the lower boundary for $k-1$, and this continues until $k = 0$. The upper boundary can also be solved using the same process described above. Figure 7 illustrates the solution process for the final state constrained global optimization strategy based on FSCDP.

To better compare and analyze with rule-based energy management, based on the simulated SOC results, the upper and lower boundaries of the terminal state x_f are set to a smaller range based on the target state. Using the boundary solving method described above, it is possible to achieve boundary solving based on terminal state constraints.

4 Results and discussion

4.1 HIL simulation platform

To validate the rationality and effectiveness of the HET energy management strategy, this paper has constructed an HIL simulation platform based on the PowerECU rapid control prototype and the NI real-time simulator. The HIL test platform connects the real-time simulator with the controller through board interfaces to facilitate communication. Once the compilation and configuration of the established vehicle model are completed, it is downloaded into the real-time simulator. Additionally, the aforementioned control strategy is downloaded into the controller to conduct HIL simulation experiments. The HIL simulation platform is illustrated in Figure 8.

4.2 Comparative analysis

The plowing operation load of the tractor is obtained from the tractor load spectrum. According to the probability distribution characteristics of the load, it is known that the tractor plowing load follows a normal distribution[42]. Based on the probability function and autocorrelation function of the load for the Dongfanghong 1804 tractor, an HET with random load plowing conditions is established. The tractor's plowing operation includes two main stages: the adjustment stage and the plowing stage. The speed during the adjustment stage is set to 3.5 km/h. To reflect the diversity of tractor implements, the plowing stage considers two speeds: 9 km/h and 6 km/h, and two load states, 100% and 80%, are set. The plowing operation conditions are shown in Figure 9.

In the HIL simulation study of the HET, the simulation research is conducted using energy management strategies based on DR and FLR. Figure 10 demonstrates the speed tracking effect, showing that the tractor effectively maintains the target speed during the plowing operation. However, due to the impact of random load fluctuations during plowing, the actual vehicle speed exhibits a certain degree of oscillation. This oscillation is primarily influenced by changes in traction resistance, and as the resistance increases, the oscillation range of the actual vehicle speed also increases. The maximum error between the actual and target speeds is 0.577 km/h, with an average error of 0.076 km/h, indicating the efficient feasibility of the hardware-in-the-loop simulation model of the hybrid electric tractor in a complex environment with varying traction resistance, meeting the accuracy requirements of the simulation.

In Figure 11, the simulation results of the operating points of the engine, P1 motor, and P2 motor are presented for the plowing operation with an initial SOC setting of 50%. The target state boundaries of the FSCDP control strategy are based on the SOC

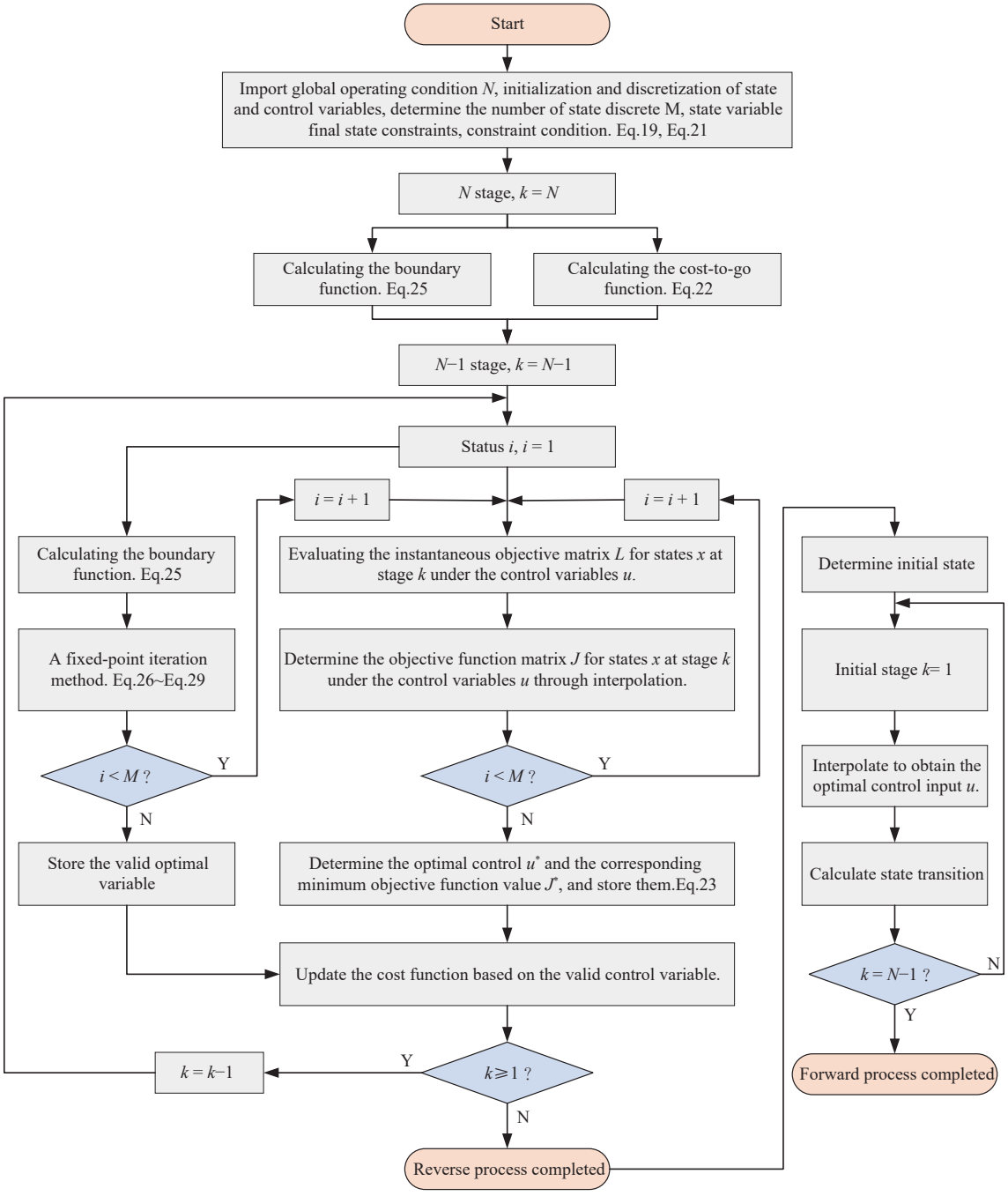

Schematic diagram of the FSCDP solution process

Figure 7 Schematic diagram of the FSCDP solution process

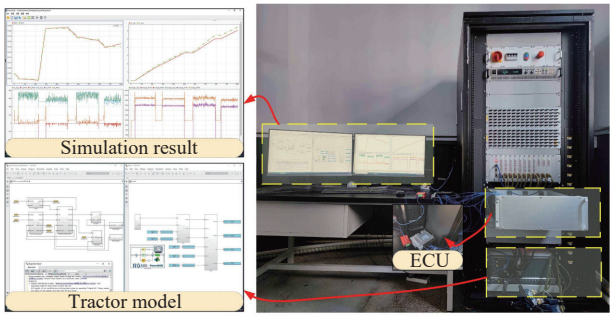

Figure 8 HIL simulation platform

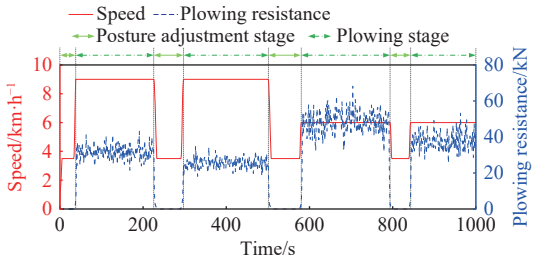

Figure 9 Plowing operation conditions

values obtained from the FLR control strategy simulation, with the boundary region set to [0.328, 0.329]. From the figure, it can be observed that under the DR control strategy, the engine operates in a larger region, the P1 motor works as a generator set in coordination with the engine according to demand, and the P2 motor mainly operates during the adjustment phase while providing additional torque beyond the maximum torque of the engine. In comparison, under the FLR control strategy, the engine's operating point tends towards a region with lower fuel consumption, the P1 motor operates similarly to the DR case, and the P2 motor can act as

a generator to absorb excess torque from the engine output or as an electric motor to assist the engine by providing additional torque. Under the FSCDP control strategy, the engine operates essentially on the optimal fuel consumption curve, and the operating ranges of P1 and P2 motors are significantly expanded, allowing them to work together more flexibly and efficiently. These results clearly demonstrate the excellent performance of the DP algorithm in energy management.

In Figure 12, the simulated energy consumption during plowing operations with different control algorithms is presented for an initial SOC of 50%. The FLR and DR control strategies exhibit consistent SOC trends during the adjustment phase. In the plowing phase, the FLR control strategy, with adjustments based on fuzzy rules, incorporates the assistance of the P2 motor. Compared to the DR control strategy, this effectively enhances the fuel economy of the tractor. Under the FSCDP control strategy, which involves backward solving and forward optimization, the variation in SOC indicates that the system can intelligently leverage the advantages of the hybrid power system based on load variations.

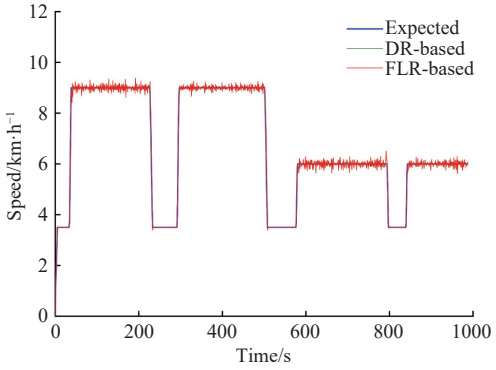

Figure 10 Comparison of actual vehicle speed and required vehicle speed in plowing conditions

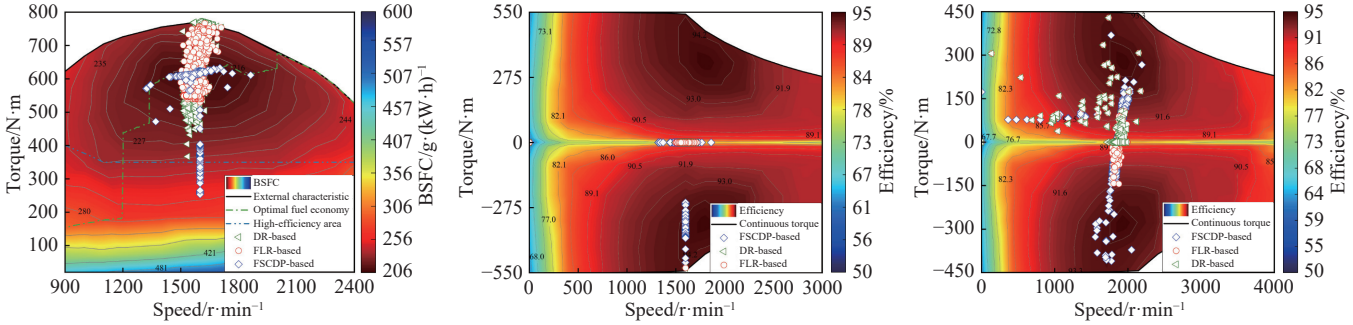

a. Engine b. P1 motor c. P2 motor

Figure 11 Operating points of the engine and motor with initial SOC at 50%

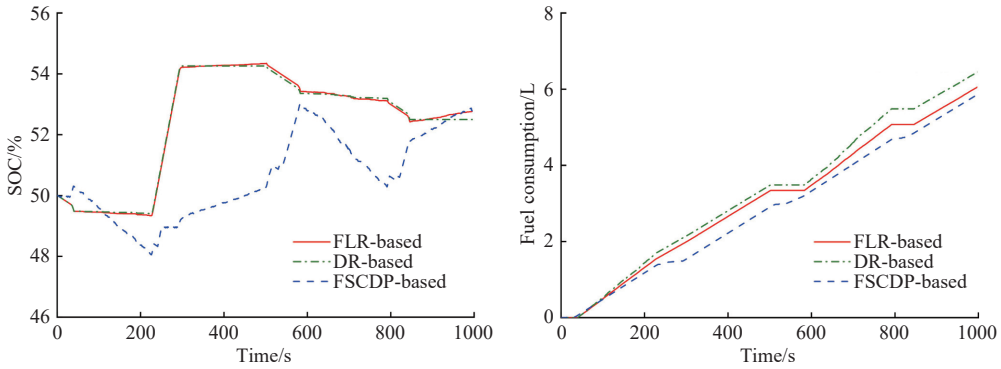

a. SOC change curve b. Fuel consumption curve

Figure 12 Energy consumption with initial SOC at 50%

Table 4 presents the comparison results of different control strategies under plowing conditions for 1000 seconds with an initial SOC set at 50%. The FLR control strategy shows a fuel consumption of 6.072 L in this scenario, with a terminal SOC of 52%. Compared to the DR control strategy, the FLR control strategy reduces fuel consumption by 6.05% while increasing the SOC value by 0.57%. Under FSCDP control, the SOC terminal value for FLR is the same as FSCDP, and fuel consumption is realized at a level of 96.6%.

Table 4 Energy consumption comparison of different control strategies with initial SOC at 50%

Control strategy	DR-based	FLR-based	FSCDP-based
Initial SOC/%	50	50	50
Final SOC/%	52.5	52.8	52.8
Fuel consumption/L	6.463	6.072	5.868

In the agricultural production process, tractors often operate under high-load conditions and may face situations with imperfect charging conditions. To verify whether the proposed control strategy can sustain power output in such an environment, simulation experiments were conducted with initial SOC values set at the lower limit of 30% and the upper limit of 80% for the traction battery pack SOC.

Figures 13 and 14 illustrate simulation results of the engine and motor operating points with initial SOC values of 30% and 80%, respectively. Comparing Figures 11, 13, and 14, it can be observed that, under different initial SOC conditions, the engine operating point distribution area for the DR control strategy remains basically consistent. In contrast, the FLR control strategy shifts the overall engine operating point upward at lower SOC and downward at higher SOC. During the adjustment phase, both control strategies employ the PE mode for operation when SOC is above 50%,

providing power, and switch to the SH mode for charging the power battery when SOC is below 50%. In comparison, the FSCDP control strategy strives to maintain the engine operating point near the optimal fuel efficiency curve at different SOC levels.

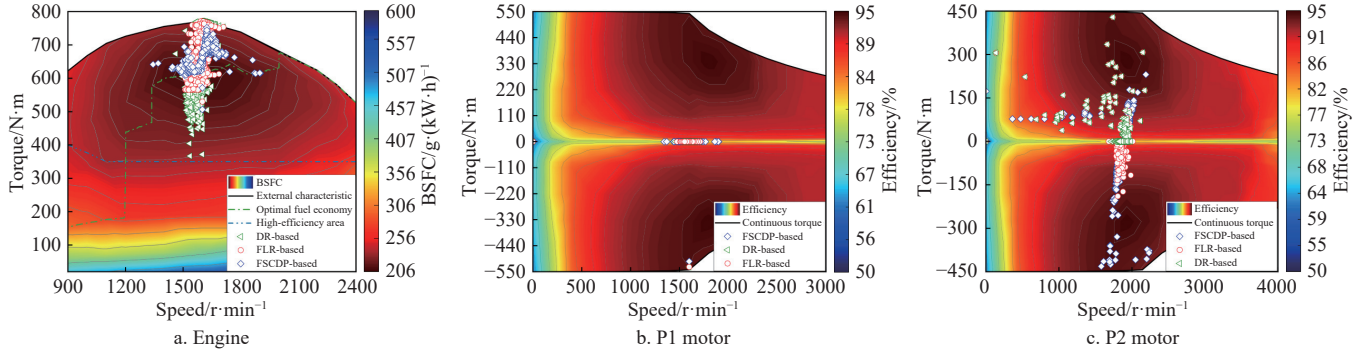

a. Engine b. P1 motor c. P2 motor

Figure 13 Operating points of the engine and motor with initial SOC at 30%

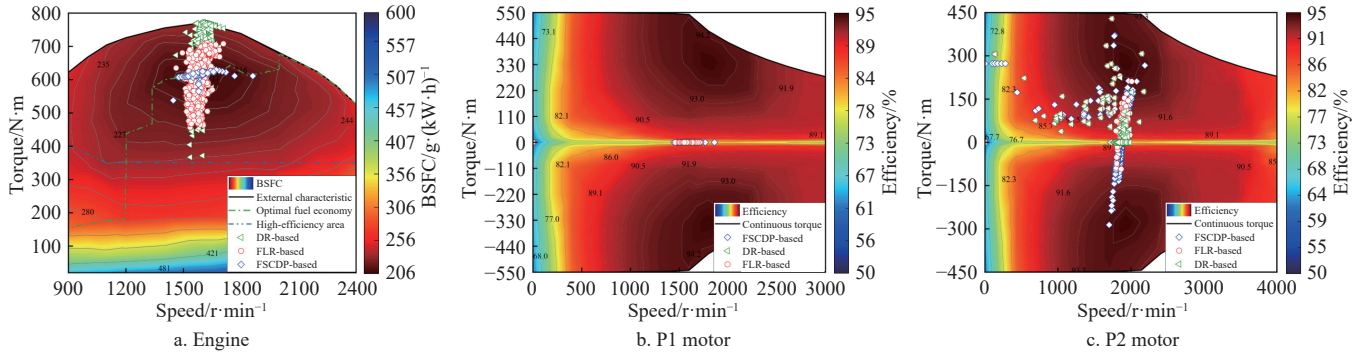

a. Engine b. P1 motor c. P2 motor

Figure 14 Operating points of the engine and motor with initial SOC at 80%

Figures 15 and 16 depict the energy consumption simulation results with initial SOC values of 30% and 80%, respectively. Both FLR and DR control strategies achieve a convergence trend of SOC towards the middle, with FLR control strategy exhibiting a faster convergence compared to the DR control strategy. Both control strategies meet the requirements for plowing conditions, maintaining the SOC of the power battery within the set upper and lower limits, ensuring the safe operation of the power battery.

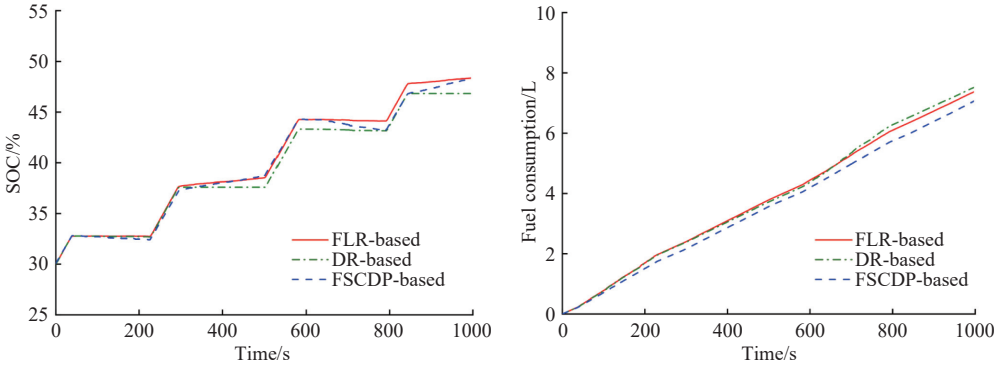

a. SOC change curve b. Fuel consumption curve

Figure 15 Energy consumption with initial SOC at 30%

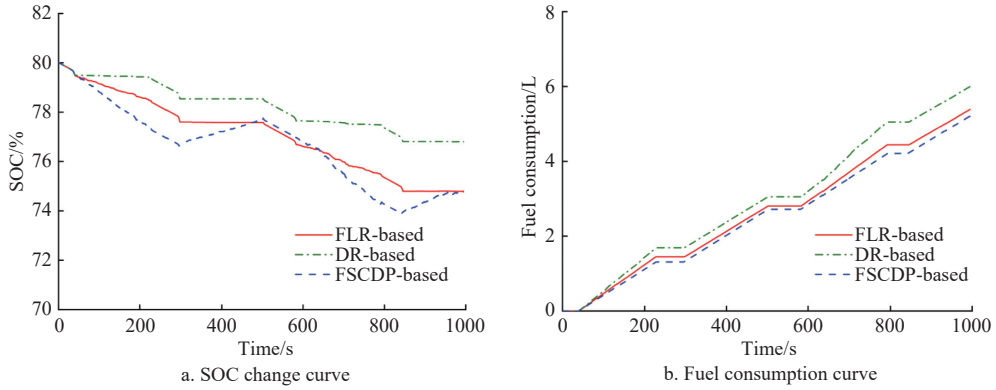

a. SOC change curve b. Fuel consumption curve

Figure 16 Energy consumption with initial SOC at 80%

Table 5 presents the comparison results for different control strategies with an initial SOC of 30%. The fuel consumption for the FLR control strategy is 7.391 L, with a final SOC of 48.4%. Compared to the DR control strategy, the fuel consumption for the FLR control strategy decreases by 1.95%, and the SOC increases by 3.42%. Under the FSCDP control, the FLR control strategy achieves a fuel consumption level of 95.8%.

Table 5 Energy consumption comparison of different control strategies with initial SOC at 30%

Control strategy	DR-based	FLR-based	FSCDP-based
Initial SOC/%	30	30	30
Final SOC/%	46.8	48.4	48.4
Fuel consumption/L	7.538	7.391	7.084

Table 6 presents the comparison results for different control strategies with an initial SOC of 80%. The fuel consumption for the FLR control strategy is 5.420 L, with a final SOC of 74.8%. Compared to the DR control strategy, the fuel consumption for the FLR control strategy decreases by 10.10%, and the SOC decreases by 3.42%. Under the FSCDP control, the FLR control strategy achieves a fuel consumption level of 96.6%.

Table 6 Energy consumption comparison of different control strategies with initial SOC at 80%

Control strategy	DR-based	FLR-based	FSCDP-based
Initial SOC/%	80	80	80
Final SOC/%	76.8	74.8	74.8
Fuel consumption/L	6.029	5.420	5.238

A comparative analysis of results under the two distinct initial SOC conditions reveals that energy management strategy efficacy is highly dependent on initial battery SOC. At 80% SOC, the FLR strategy achieves a 10.10% fuel reduction compared to DR strategy, while at 30% SOC, this advantage diminishes to only 1.95%. This disparity occurs because high SOC enables electric-dominant operation, whereas low SOC necessitates prioritizing battery charging over fuel economy. These findings indicate that adaptive energy management systems must implement SOC-dependent control parameters to optimize energy distribution across all operating conditions.

5 Conclusions

(1) To enhance the fuel economy of the SPHET, a dynamic model for passive unit operation of the SPHET was developed based on tractor operations and the working mode of the SPHET. A real-time energy management strategy for the HET is proposed, utilizing FLR. To assess more accurately the control strategy's superiority, an energy management strategy for the SPHET based on FSCDP was introduced. An HIL simulation platform for the SPHET energy management control strategy was established to validate the feasibility of the energy management control strategy and the sustained power output capability of the SPHET.

(2) Simulations were conducted under plowing conditions for different energy management strategies, with the initial SOC set at 50%. Compared to the DR control strategy, the FLR control strategy performed exceptionally well under plowing conditions, reducing fuel consumption by 6.05%, and increasing SOC by 0.57%. Compared to the FSCDP-based control strategy, both control strategies yielded the same final SOC values, and the fuel consumption of the FLR control strategy reached 96.6% of that achieved by FSCDP.

(3) Through comparative analysis of simulations under plowing conditions for the SPHET with different initial SOC values and energy management control strategies, the FSCDP-based energy management control strategy achieved globally optimal fuel economy through the DP algorithm. This approach employed a boundary-solving method with constrained termination states, effectively mitigating the impact of differences in final SOC on the comparison of control strategy superiority. The FLR control strategy, adjusted by fuzzy logic, effectively improved the fuel economy of the tractor compared to the DR control strategy. Both control strategies met the requirements for plowing conditions, maintaining a certain level of charge in the power battery, and ensuring the safe operation of the power battery.

This study was limited by the absence of physical vehicle validation, as all results were derived exclusively from simulation and HIL simulation platforms. Future research will implement advanced intelligent algorithms and conduct comprehensive field validation using a prototype SPHET to verify strategy effectiveness under real-world agricultural operating conditions.

Acknowledgements

This research was funded by the China National Machinery Industry Corporation Youth Science and Technology Fund (Grant No. QNJJ-ZD-2022-03) and the National Natural Science Foundation of China (Grant No. U23A20340).

[References]

[1] Moreda G P, Muñoz-García M A, Barreiro P. High voltage electrification of tractor and agricultural machinery – A review. Energy Conversion and Management, 2016; 115: 117–131.

[2] Scolaro E, Beligoj M, Estevez M P, Alberti L, Renzi M, Mattetti M. Electrification of agricultural machinery: A review. IEEE Access, 2021; 9: 164520–164541.

[3] Bie P J, Ji L, Cui H X, Li G, Liu S L, Yuan Y, et al. A review and evaluation of nonroad diesel mobile machinery emission control in China. Journal of Environmental Sciences, 2023; 123: 30–40.

[4] Liu M N, Lei S H, Zhao J H, Meng Z J, Zhao C J, Xu L Y. Review of development process and research status of electric tractors. Transactions of the CSAM, 2022; 53(S1): 348–364.

[5] Liu M N, Li Y Y, Xu L Y, Wang Y T, Zhao J H. General modeling and energy management optimization for the fuel cell electric tractor with mechanical shunt type. Computers and Electronics in Agriculture, 2023; 213: 108178.

[6] Xu L Y, Zhang J J, Yan X H, Zhao S X, Wu Y W, Liu M N. Review of research for agricultural equipment electrification technology. Transactions of the CSAM, 2023; 54(9): 1–12.

[7] Gao H S, Xue J L. Modeling and economic assessment of electric transformation of agricultural tractors fueled with diesel. Sustainable Energy Technologies and Assessments, 2020; 39: 100697.

[8] Nordelöf A, Messagie M, Tillman A M, Söderman M J, Mierlo J V. Environmental impacts of hybrid, plug-in hybrid, and battery electric vehicles—what can we learn from life cycle assessment?. International Journal of Life Cycle Assessment, 2014; 19(11): 1866–1890.

[9] Zhuang W C, Li S B, Zhang X W, Kum D, Song Z Y, Yin G D, et al. A survey of powertrain configuration studies on hybrid electric vehicles. Applied Energy, 2020; 262: 114553.

[10] Saiteja P, Ashok B. Critical review on structural architecture, energy control strategies and development process towards optimal energy management in hybrid vehicles. Renewable and Sustainable Energy Reviews, 2022; 157: 112038.

[11] He H W, Meng X F. A review on energy management technology of hybrid electric vehicles. Transactions of Beijing Institute of Technology, 2022; 42(8): 773–783.

[12] Peng J K, He H W, Xiong R. Rule based energy management strategy for a series–parallel plug-in hybrid electric bus optimized by dynamic

programming. Applied Energy, 2017; 185: 1633–1643.
[13] Xu L Y, Zhang J J, Liu M N, Zhou Z L, Liu C Q. Control algorithm and energy management strategy for extended range electric tractors. Int J Agric & Biol Eng, 2017; 10(5): 35–44.
[14] Kang H, Jung D, Kim M, Min K. Study of energy management strategy considering various working modes of plug-in hybrid electric tractor. Transactions of the Korean Society of Mechanical Engineers B, 2013; 37(2): 181–186.
[15] Lee D H, Kim Y J, Choi C H, Chung S O, Inoue E, Okayasu T. Development of a parallel hybrid system for agricultural tractors. Journal of the Faculty of Agriculture Kyushu University, 2017; 62(1): 137–144.
[16] Jia C, Qiao W, Qu L Y. Modeling and control of hybrid electric vehicles: A case study for agricultural tractors. 2018 IEEE Vehicle Power and Propulsion Conference (VPPC). 2018; 1–6. DOI: 10.1109/VPPC.2018.8604997.
[17] Wang L M, Wang S M, Song Z H. Control strategy and startup method of extended range electric tractors. Transactions of the CSAM, 2018; 49(S1): 486–491.
[18] Mocera F, Somà A. Analysis of a parallel hybrid electric tractor for agricultural applications. Energies, 2020; 13(12): 3055.
[19] Mocera F, Martini V. Numerical performance investigation of a hybrid eCVT specialized agricultural tractor. Applied Sciences-Basel, 2022; 12(5): 2438.
[20] Rossi C, Pontara D, Falcomer C, Bertoldi M, Mandrioli R. A hybrid–electric driveline for agricultural tractors based on an e-CVT power-split transmission. Energies, 2021; 14(21): 6912.
[21] Wu Z K, Wang J Z, Xing Y Z, Li S S, Yi J G, Zhao C M. Energy management of sowing unit for extended-range electric tractor based on improved CD-CS fuzzy rules. Agriculture-Basel, 2023; 13(7): 1303.
[22] Dou H S, Wei H Q, Zhang Y T, Ai Q. Configuration design and optimal energy management for coupled-split powertrain tractor. Machines, 2022; 10(12): 1175.
[23] Zhang J J, Feng G H, Xu L Y, Wang W, Yan X H, Liu M N. Energy-saving control of hybrid tractor based on Pontryagin's minimum principle. Transactions of the CSAM, 2023; 54(5): 396–406.
[24] Zhang J J, Feng G H, Yan X H, He Y D, Liu M N, Xu L Y. Cooperative control method considering efficiency and tracking performance for unmanned hybrid tractor based on rotary tillage prediction. Energy, 2024; 288: 129874.
[25] Wang Z Z, Zhou J, Wang X. Research of energy management model for extended-range electric rotary-tilling tractor. Transactions of the CSAM, 2023; 54(4): 428–438.
[26] Zhu Z, Zeng L X, Ling Y G, Chen L, Zou R, Cai Y F. Adaptive energy management strategy for hybrid tractors based on condition prediction. Journal of Xi'an Jiaotong University, 2023; 57(12): 201–210.
[27] Flint J, Zhang D M, Xu P. Preliminary market analysis for a new hybrid electric farm tractor. Proceedings of the 2014 International Conference on Global Economy, Commerce and Service Science. Phuket, Thailand, 2014. DOI: 10.2991/gecss-14.2014.25
[28] Harselaar W V, Schreuders N, Hofman T, Rinderknecht S. Improved implementation of dynamic programming on the example of hybrid electric vehicle control. IFAC-PapersOnLine, 2019; 52(5): 147–152.
[29] Hu J Y, Li J Q, Hu Z Y, Xu L F, Ouyang M. Power distribution strategy of a dual-engine system for heavy-duty hybrid electric vehicles using dynamic programming. Energy, 2021; 215: 118851.
[30] Lü X, Li S W, He X H, Xie S J, Xu Y Z, Fang J. Hybrid electric vehicles: A review of energy management strategies based on model predictive control. Journal of Energy Storage, 2022; 56: 106112.
[31] Deng X T, Zhu S H, Gao H S, Zhang Y. Design theory and method for drive train of hybrid electric tractor. Transactions of the CSAM, 2012; 43(8): 24–31, 36.
[32] Xu L Y, Liu M N, Zhou Z L. Design of drive system for series hybrid electric tractor. Transactions of the CSAE, 2014; 30(9): 11–18.
[33] Zhu Z, Yang Y P, Wang D Q, Cai Y F, Lai L H. Energy saving performance of agricultural tractor equipped with mechanic-electronic-hydraulic powertrain system. Agriculture-Basel, 2022; 12(3): 436.
[34] Li X Z, Zhang M Z, Yan X H, Liu M N, Xu L Y. Power allocation strategy for fuel cell distributed drive electric tractor based on adaptive multi-resolution analysis theory. Energy, 2023; 284: 129350.
[35] Tiwari V K, Pandey K P, Pranav P K. A review on traction prediction equations. Journal of Terramechanics, 2010; 47(3): 191–199.
[36] Zhao J H, Liu M N, Xu L Y, Yu S, Xie P K. Prediction model and experiment on tractive performance of four-wheel drive tractor. Transactions of the CSAM, 2023; 54(9): 439–447.
[37] Bellman R. Dynamic programming. Science, 1966; 153(3731): 34–37.
[38] Maino C, Misul D, Musa A, Spessa E. Optimal mesh discretization of the dynamic programming for hybrid electric vehicles. Applied Energy, 2021; 292: 116920. DOI: 10.1016/j.apenergy.2021.116920.
[39] Sundström O, Guzzella L. A generic dynamic programming Matlab function. 2009 IEEE International Conference on Control Applications. 2009; 1625–1630. DOI: 10.1109/CCA.2009.5281131.
[40] Sundström O, Ambühl D, Guzzella L. On implementation of dynamic programming for optimal control problems with final state constraints. Oil & Gas Science and Technology - Rev. IFP Energies Nouvelles, 2010; 65(1): 91–102. DOI: 10.2516/ogst/2009020.
[41] Zeng X H, Wang Y, Yang N N, Song D F, Li G H. Global optimization algorithm for planetary hybrid powertrain based on constrained termination state. Automotive Engineering, 2019; 41(3): 239–244, 258.
[42] Fang Z H, Zhou Z L, Yang T Z, Zhang W C, Zhang J, Guan X Q. The statistical characteristics of the engine load during plowing and rotary tillage operations. Transactions of the CSAE, 2000; 16(4): 85–87.